

PAPER • OPEN ACCESS

Identifying muon sites “by eye” in KPF_6 and KBF_4

To cite this article: J M Wilkinson *et al* 2023 *J. Phys.: Conf. Ser.* **2462** 012007

View the [article online](#) for updates and enhancements.

You may also like

- [Pressure-induced superconductivity in CrAs and MnP](#)
Jinguang Cheng and Jianlin Luo
- [Muon spin relaxation study on itinerant ferromagnet CeCrGe₃ and the effect of Ti substitution on magnetism of CeCrGe₃](#)
Debarchan Das, A Bhattacharyya, V K Anand et al.
- [Nodeless superconductivity in the cage-type superconductor Sc₂Ru₆Sn₁₀ with preserved time-reversal symmetry](#)
D Kumar, C N Kuo, F Astuti et al.

Identifying muon sites “by eye” in KPF_6 and KBF_4

J M Wilkinson^{1,3}, F Lang^{1,3}, P J Baker², S P Cottrell², and
S J Blundell¹

¹ Clarendon Laboratory, University of Oxford, Parks Road, Oxford, Oxfordshire, OX1 0PU

² STFC-ISIS Facility, Rutherford Appleton Laboratory, Harwell Campus, Chilton, Oxfordshire, OX11 0QX

E-mail: john.wilkinson@stfc.ac.uk

Abstract. Molecular magnets are one of the key research themes of μSR , but locating the muon stopping site in these compounds using density functional theory is often very challenging as their unit cells tend to contain a very large number of atoms. Nevertheless, many molecular magnets contain the $[\text{PF}_6]^-$ and $[\text{BF}_4]^-$ molecular ions, which, due to their fluorine nuclei, produce a distinctive μSR spectrum, which can give information about the muon stopping site. This paper details the calculation of the muon sites in the much simpler materials KPF_6 and KBF_4 , providing insights which can be applied to situations where these molecular ions are found in complicated molecular magnets.

1. Introduction

One of the principal uses of μSR is to measure magnetic materials, but the magnetic field the muon observes depends strongly on the muon stopping site, and the challenges of calculating this can often prohibit a full quantitative analysis of the data. Although $\text{DFT}+\mu$ has been very successful in locating muon stopping sites in many cases [1, 2], the fact that much of the rich physics of the most exciting quantum materials arises due to their d and f electrons means that performing such calculations can take a very long time and is therefore unfeasible, even with the pseudoisation of the core electrons. It is therefore helpful to see whether, in some materials, the muon stopping site can be determined by observing key features of the data, and using these to narrow down the muon stopping site. This would provide an independent check on $\text{DFT}+\mu$ calculations or even rendering its use redundant by simply identifying the stopping site “by eye”.

This paper will detail the analysis of two compounds: KPF_6 and KBF_4 . These compounds contain the hexafluorophosphate ion ($[\text{PF}_6]^-$) and the tetrafluoroborate ion ($[\text{BF}_4]^-$), both of which are often found in molecular magnets [3–7]. By studying them in these compounds where the cation has a very limited effect on the μSR spectrum (as all isotopes of K have a very low nuclear moment) one should be able to use the information gained from the analysis of these $\text{F}-\mu-\text{F}$ states to gain insight into the muon site in more complex molecular compounds containing these ions.

³ Current address: STFC-ISIS Facility, Rutherford Appleton Laboratory, Harwell Campus, Chilton, Oxfordshire, OX11 0QX



2. KPF₆

KPF₆ consists of octahedral [PF₆][−] ions intercalated with K⁺ ions. The crystal structure of KPF₆ has four phases, I–IV, as described in Refs. [8, 9], but in this study the compound was assumed to be in the trigonal phase IV, which is depicted in Figure 1a. The positively charged muon can be assumed to be in between two fluorines which are initially relatively close together (so that the Coulomb forces due to the muon at the fluoride ions in their original positions are strong enough to sufficiently displace them) to form an F–μ–F state. There are therefore two categories of states the muon can form in this compound: “intra-octahedra” states, where the F–μ–F bond is formed between two fluorines in the same [PF₆][−] octahedron, and “inter-octahedra” states, where the muon bonds to two fluorines on different [PF₆][−] octahedra.

2.1. Muon site determination

We calculated the muon polarisation for muons in various sites using the dipole-dipole Hamiltonian,

$$\mathcal{H} = \sum_{i < j} \frac{\mu_0 \gamma_i \gamma_j}{4\pi |\mathbf{r}_{ij}|^3} (\mathbf{s}_i \cdot \mathbf{s}_j - 3(\mathbf{s}_i \cdot \hat{\mathbf{r}}_i)(\mathbf{s}_j \cdot \hat{\mathbf{r}}_j)), \quad (1)$$

cutting off the Hilbert space when the matrices were of size 2048 × 2048. We chose the nuclei to be included in the calculation by calculating the size of the interaction between the muon and each of the nuclei surrounding the muon as $\frac{\mu}{r^3}$ [where μ is the nuclear moment and r is the distance between the muon and the nucleus], selecting the nuclei with the ten largest values of this figure of merit. Figure 1b shows the muon polarisation one would expect from muons in various sites. In this figure, the muon-induced distortions are assumed to only be felt by the nearest-neighbour fluorines, and are assumed to be in a radial direction⁴. The nearest-neighbour F–μ distance was set to be 1.20 Å for every muon site, which is a rough estimate of the expected distance based on previously measured F–μ–F states.

From this figure, it is clear that a change in muon site has a significant effect on the μSR data: each of the states produces a muon polarisation which is visually distinct, even though they are *all* F–μ–F states. These different muon sites would certainly not be distinguishable to any significant extent if the approach of modelling the relaxation by a stretched exponential function was used, as the main difference between these sites is the nature of the muon’s decohering environment of surrounding nuclear spins. By comparing the data in Figure 2 to the states in Figure 1b, it is clear that the muon state which most closely matches the data is the light blue inter-octahedra state. This is likely because the P atom in the centre of the [PF₆][−] ion has a slight positive charge, which repels the muon and ensures only inter-octahedra muon sites are realised.

In order to confirm this site, and to predict the lattice distortions, we also performed DFT+μ calculations on KPF₆. As the rough location of the muon stopping site was determined previously, only one DFT relaxation calculation was required, as it was not necessary to place the muon in lots of random locations in the crystal structure. A supercell was constructed from 2 × 2 × 2 conventional unit cells, and the muon was placed in an inter-octahedral position similar to that determined from the muon polarisation, and, as usual, the cell was given a charge of +|e| to represent the charge state of the muon. The DFT+μ calculation predicts that the muon strongly distorts its nearest-neighbour fluorines, but the distortions of the further ions are to a lesser (but not negligible) extent. The DFT+μ result also predicted a slightly off-centre site: the distance between the muon and the two nearest fluorine atoms (r_{nn1} and r_{nn2}) was 1.07 Å and 1.25 Å respectively.

⁴ These assumptions also mean that the F–μ–F bond angle is different for all the sites, but by comparing the two sites closest to the centre of the quadrilateral of the four fluorines one can see that the overall environment of the muon has the greatest effect, as these two have a very similar muon polarisation but different F–μ–F bond angles.

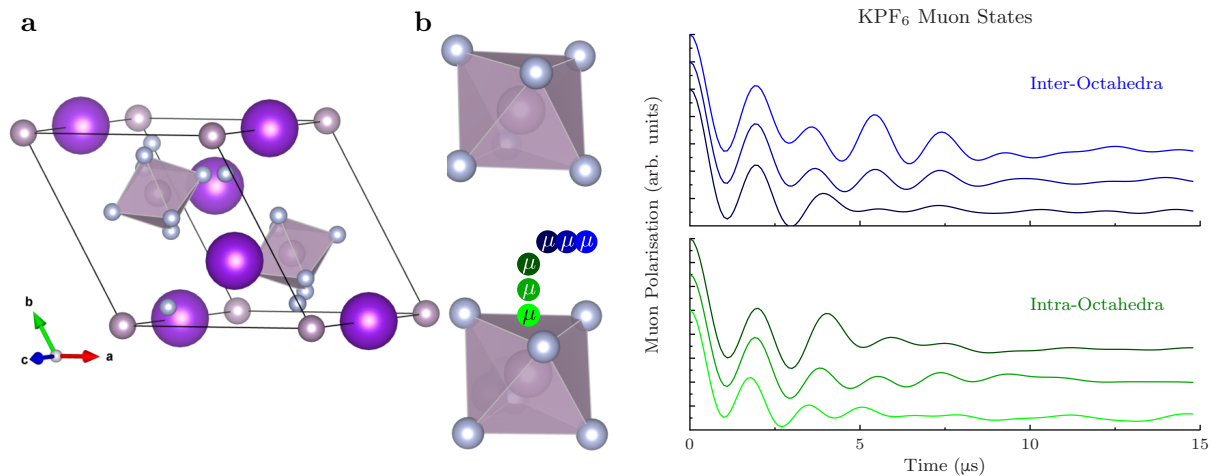


Figure 1. Muon states in KPF_6 . **a** depicts the crystal structure of KPF_6 , with fluorine, phosphorus and potassium atoms depicted as grey, lilac and purple spheres respectively. **b** shows the expected muon polarisation calculated for the muons in the positions as shown on the diagram in the left side of the subfigure, with the colour of the muons matching the corresponding muon polarisation on the right hand side. The octahedra depicted are the two shown in the conventional unit cell in **a**, looking in the $-b$ direction.

2.2. Results and analysis

A polycrystalline sample of KPF_6 was obtained commercially, and wrapped in 25 μm Ag foil. The sample was initially placed in an X-Ray diffractometer, and we found that the purity was over 90%, and none of the impurities significantly affected the μSR spectrum. We placed this sample in the EMU spectrometer at ISIS [10], and collected 1453 million muon decay events at 10 K, and 182 million events at temperatures 20, 30, and 40 K.

With the DFT+ μ results in mind, we fitted the μSR data to the function

$$A(t) = A_{\text{rel}}P_{\mu}(r_{\text{nn}}, r_{\text{disp}}; t) + A_{\text{imp}}e^{-\lambda t} + A_{\text{bg}}, \quad (2)$$

where the first term represents the muons in the F- μ -F state in KPF_6 , and r_{nn} is the distance between the muon and the two nearest neighbour fluorines⁵, r_{disp} is the displacement of the muon from the site determined by DFT+ μ in the direction perpendicular to the line joining the two nearest-neighbours (i.e. increasing this moves the muon from the light blue state in Figure 1b to the darker blue), a parameter which in effect also adjusts the F- μ -F bond angle. Owing to the particularly high statistics of our dataset, particularly at 10 K, we used a large Hilbert space to calculate $P_{\mu}(\dots; t)$, with the matrices being of dimension 4096×4096 , and the eight furthest nuclei from the muon within this cutoff were rescaled by a factor ζ_8 , calculated from the DFT+ μ results using the second moment of the dipole field distribution (using the methods detailed in Refs. [11–13]) and this was *not* used as a fitting parameter. The second term in the fitting function ($A_{\text{imp}}e^{-\lambda t}$) models muons stopping in the various impurities in the sample, with the small nuclear moments causing a slow relaxation. The final term (A_{bg}) was included to model the small Ag nuclear moments in the sample holder, a term which is small because the very large KPF_6 sample covered the vast majority of the beam spot. The value of these amplitudes were $A_{\text{rel}} = 11.76(3)\%$, $A_{\text{imp}} = 1.223(4)\%$ and $A_{\text{bg}} = 1.87(1)\%$, and were fixed

⁵ Fits were also attempted which allowed the two nearest-neighbours to the muon to have a different distances, but both values always converged to be the same, so were fixed as r_{nn} .

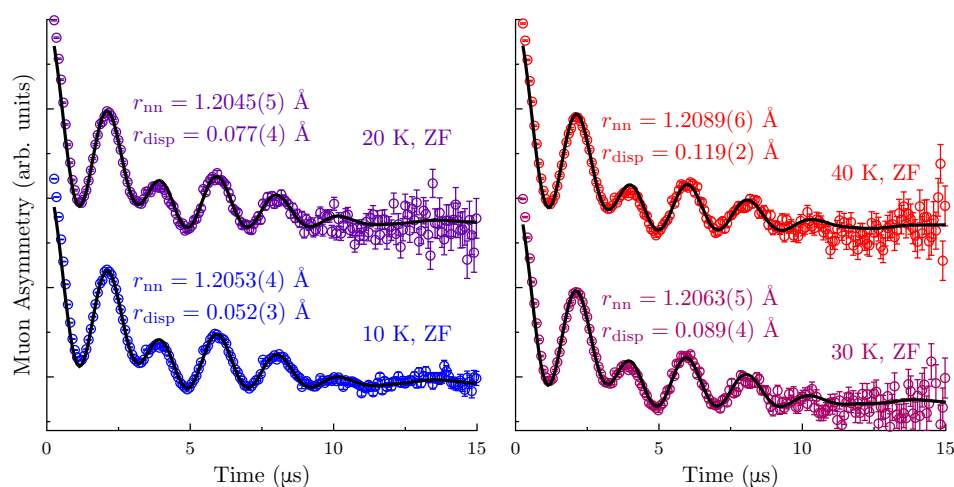


Figure 2. Fits of the KPF_6 EMU data, using Equation (2). The fitted parameters r_{nn} and r_{disp} are shown next to the relevant plot for each temperature.

in every fit. The fits are shown in Figure 2, which depicts the impressive agreement between the data and the model, and the values of the fitting parameters r_{nn} and r_{disp} . These results also show that the nearest-neighbour μ -F distance increases slightly with temperature. The origin of this is unclear, not least because the random error for each of these values is close to the change of the values between the temperatures. Nevertheless, thermal expansion might be a suitable explanation for this: the coefficient of thermal expansion for $[\text{PF}_6]^-$ -containing compounds tends to be of the order of 10^{-5} K^{-1} [14], consistent with the order of magnitude of the changes in r_{nn} , but as only four temperatures were measured, it is not possible to conclusively determine this as the cause. The variation of r_{disp} with temperature is too large to be due to thermal expansion effects alone. A close inspection of Figure 1b suggests that increasing r_{disp} has the effect of increasing the relaxation, which would also happen if the muon is slowly diffusing at higher temperatures, an effect which is beyond the scope of this study.

3. KBF_4

KBF_4 consists of tetrahedral $[\text{BF}_4]^-$ ions intercalated with K^+ , in the space group $Pnma$ [15], as shown in Figure 3a. The fluorines occupy three distinct Wyckoff sites, labelled in the figure as F1–3, all of which have a multiplicity of 4.

3.1. Muon site determination

As the fluorine atoms occupy three different Wyckoff sites, determining which site (or sites) the muon stops in is best achieved by DFT+ μ . We placed muons in between every pair of fluorines less than 3.3 Å apart in a supercell consisting of $1 \times 2 \times 2$ conventional unit cells, again giving the supercell a charge of $+|e|$ due to the muon's charge state, and these were all relaxed until the forces on the atoms fell below a certain threshold. The final muon sites are listed in Table 1, analysed in terms of the total energy of the relaxed supercell.

From these DFT+ μ results, we can determine several properties of the KBF_4 muon site: firstly, there is an absence of any muon sites which are in between two fluorines of type F1 and two of type F2. The closest distance between two F1s (where a line can be drawn between them without touching the other atoms) is 4.21 Å, and for the F2s this is 3.41 Å, which are both larger than the initial distance between all the other pairs of fluorines, suggesting these sites do

Nearest-neighbour fluorines	Number of DFT runs	ΔE (meV)
F1 \leftrightarrow F2	6	0
F2 \leftrightarrow F3	2	83
F3 \leftrightarrow F3	4	100–120
F1 \leftrightarrow F3	4	100–200

Table 1. KBF_4 DFT+ μ results. Each pair of fluorines which had a muon site predicted by DFT+ μ is shown, alongside the number of DFT+ μ calculations predicting each of these sites. The range of energies of the relaxed supercells for each site is also shown (ΔE is the difference in energy between the site with the lowest energy and the site in question).

not minimise the total energy because very large perturbations of the crystal would be required to form such F– μ –F states⁶. Secondly, *all* of the states are formed between fluorines on different tetrahedra (“inter-tetrahedra”), analogous to the situation in KPF_6 discussed previously.

As each of the states predicted by DFT+ μ have the muon in a different environment, each state will give rise to a different muon polarisation. Therefore, to investigate the most likely muon site, we calculated the muon polarisation for muons in each of the sites in Table 1. Boron has two isotopes, both of which have spin $I > \frac{1}{2}$, making it necessary to include both dipolar and quadrupolar terms in the Hamiltonian. Therefore we calculated the muon polarisation using a Hamiltonian composed of the sum of Equation (1) and

$$\mathcal{H}_Q = \sum_{i \in B} \frac{eQ(1 + \gamma_\infty)}{\hbar 2I(2I - 1)} \sum_{\alpha, \beta \in \{x, y, z\}} V_{\alpha\beta}^i \hat{I}_\alpha^i \hat{I}_\beta^i, \quad (3)$$

where the sum over $i \in B$ is over the boron nuclei only. The external electric field gradient (EFG) $V_{\alpha\beta}^i$ at the site of the i th boron nucleus (with spin operator \mathbf{I}^i) due to external charges q_j , was calculated using a point-charge model (to achieve this, we modelled the charge state of the boron to be +3, despite the bond between the fluorine and boron being of a covalent character). A boron in this charge state gives rise to an anti-shielding factor γ_∞ of around -0.144 , assuming an average of the values reported by various sources [16–19]. To take into account both the boron isotopes, we calculated the total muon polarisation as a weighted sum of the muon polarisation due to muons stopping in sites surrounded by each combination of boron isotopes, i.e. $P_\mu(t) = \sum_i w^i P_\mu^i(t)$, where the superscript i denotes the combination of isotopes used in the Hamiltonian to calculate the muon polarisation $P_\mu^i(t)$. The term w^i is a weighting factor, which is calculated as a product of the abundances of all the nuclei used to calculate $P_\mu^i(t)$. As a first step, we chose to cut off the Hilbert space when the matrices were of size 4096×4096 (sufficiently large to include enough nuclei to produce many of the key features of the muon polarisation, while being small enough to not take too long to compute), selecting the specific nuclei involved in the calculation in a similar way as was done for KPF_6 . For this initial investigation, we did not rescale any interactions to take into account the infinite crystal, as a poor choice of the number of nearest-neighbours to rescale is likely to result in the spectrum becoming distorted. The predicted muon polarisations from the four possible muon sites determined by DFT are plotted in Figure 3b.

⁶ Of course, all the initial muon sites (before relaxation) were between two fluorines closer than 3.3 \AA , which excluded all F1 \leftrightarrow F1 and F2 \leftrightarrow F2 sites – but if these sites have a large enough potential minimum, the relaxation calculation ought to have found them.

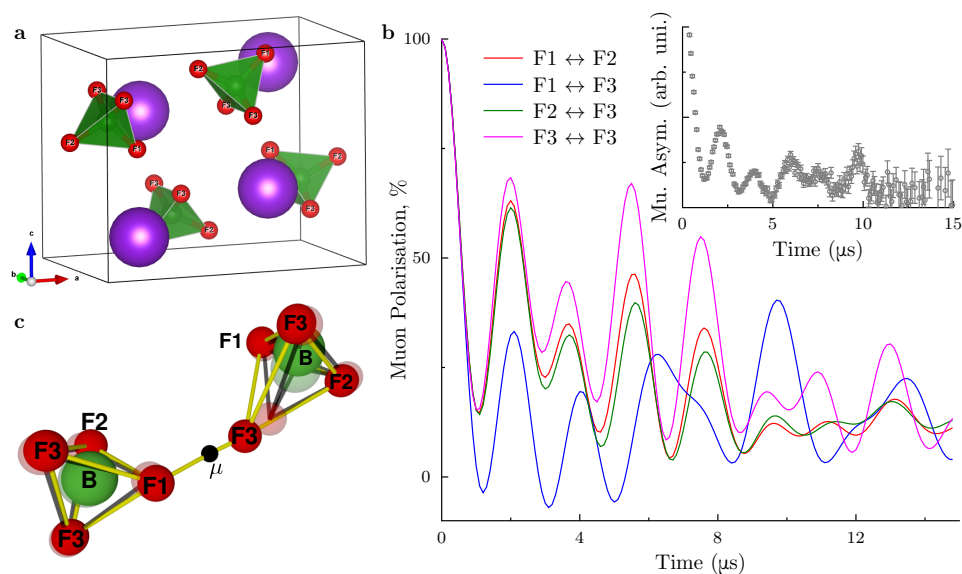


Figure 3. Muon states in KBF_4 . **a** depicts the crystal structure of KBF_4 , and **b** shows the muon polarisation expected from muons in all four potential muon states calculated with $\text{DFT}+\mu$. Inset: The muon asymmetry data from the KBF_4 sample. **c** shows the Muon-induced perturbations in KBF_4 , predicted by the $\text{F1}\leftrightarrow\text{F3}$ state. The muon is represented by the black sphere, fluorine by the red and boron by the green sphere. Distorted (undistorted) positions are shown as solid (translucent) spheres, and the lines connecting the spheres are guides to the eye. The potassium ions are not shown for clarity.

By inspecting Figure 3b, comparing each of the muon polarisations to the data (in the inset) shows that the muon site is clearly of the type $\text{F1}\leftrightarrow\text{F3}$, despite the results from the $\text{DFT}+\mu$ calculations suggesting a different muon site. This muon site is highly unusual, as some of the fluorines move considerably from their original positions, as is shown in Figure 3c. In this figure, it can be seen that the muon's perturbation pulls the nearest-neighbour F3 atom away from its $[\text{BF}_4]^-$ complex, which then makes the boron move towards its remaining three fluorides (F1, F2 and the other F3), becoming in effect a neutral planar BF_3 ion. The other $[\text{BF}_4]^-$ ion is affected far less by the muon perturbations, and all of its constituents remain in a similar location relative to each other, but all have moved slightly towards the muon.

BF_3 is a Lewis acid, which is known to accept an F^- ion to form the $[\text{BF}_4]^-$ ion. A muon has the effect of reversing this process, removing an F^- ion from the $[\text{BF}_4]^-$ ion. This is similar to the way in which the Lewis bases HCN [20] and NH_3 [21] interact with BF_3 , with the $\mu\text{-F}$ complex acting as a Lewis base in this case.

The muon state depicted in Figure 3c has many atoms which are perturbed, meaning that to get a full understanding of this the muon polarisation needs to be calculated with a larger Hilbert space than what was used for KPF_6 . To this end, we cut off the Hilbert space when the size of the matrices reached 12544×12544 for the fitting of the μSR asymmetry data (this meant the calculation included the muon, seven fluorines and both borons, even if they are both the isotope with the greater spin (^{10}B), which has $I = 3$).

To model the effects of all the nuclei in the sample affecting the muon's polarisation, we rescaled the distances of the nuclei from the muon for those more distant than its two nearest-neighbours to take into account the second dipole moment of the infinite lattice. However, the fact that boron has two isotopes means that the calculation of this rescaling factor (ζ_7) needs

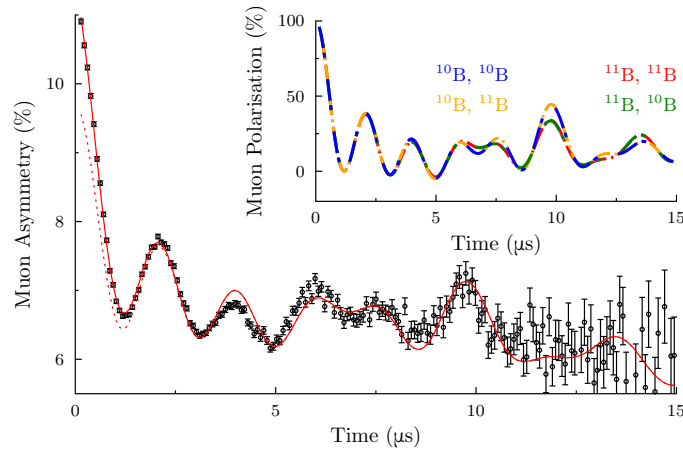


Figure 4. KBF_4 μSR fits. The main plot shows the fit of the muon data to Equation (4). The inset shows the muon polarisation functions realised when the nearest and next-nearest borons to the muon are of type ^{10}B or ^{11}B .

to be done with care: for each of the isotope combinations i , the second moment of the dipolar field distribution was calculated using broadly the same approach as for KPF_6 , with the key difference being that this needed to be calculated four times (once for each of the combinations of boron isotopes), *and* the second moment of the spins beyond those accounted for explicitly in the dipole-dipole Hamiltonian was treated as an average of that of both boron isotopes, weighted by their abundances. Therefore, there are four different values of this rescaling factor, which varies from 0.8992 (if both borons are ^{10}B) to 0.9085 (if both borons are ^{11}B).

3.2. Results and analysis

A polycrystalline sample of KBF_4 was obtained commercially, and wrapped in 25 μm Ag foil. This sample was also placed into an X-ray diffractometer and was found to have a purity of around 90 %, with the main impurities being KN_3 and KNO_3 . This sample was placed into the MuSR spectrometer at ISIS, and around 800 million muon decay events were measured at a temperature of 10 K.

We fitted the KBF_4 data with the function

$$A(t) = A_{\text{rel}}P_{\mu}(r_{\text{nn1}}, r_{\text{nn2}}; t) + A_{\text{imp}}e^{-\lambda_{\text{imp}}t} + A_{\text{bg}}e^{-(\sigma t)^2}, \quad (4)$$

a similar function to that used for KPF_6 . The first term represents the muons stopped in KBF_4 and evolving as described in the previous section, and the second term represents the muons stopping in impurities and causing their polarisation to decay exponentially (this is inevitably a phenomenological relaxation function, as the X-ray data could not conclusively determine what the impurities were). The final term is a Gaussian decay due to muons stopping in the Ag sample holder. The muon polarisation for the muon stopping in KBF_4 uses values for ζ_7 calculated from our DFT+ μ results, because having this as a variable parameter would require the introduction of four additional fitting parameters (due to the boron isotope combinations), all of which would change the muon polarisation a similar way resulting in many local minima for the fit.

The fit was in excellent agreement with the data, as depicted in Figure 4. The isotope combinations are also depicted in the inset, showing the significant effect of substituting the nearest boron nucleus on the muon polarisation (^{11}B has a larger nuclear moment

that ^{10}B , explaining the more significant relaxation which occurs if the nearest boron atom to the muon is of this species). The nearest-neighbour distances to the muon were $r_{\text{nn1}} = 1.077(1) \text{ \AA}$ and $r_{\text{nn2}} = 1.489(6) \text{ \AA}$, very close to the values obtained by DFT+ μ of 0.908 \AA and 1.456 \AA respectively. The amplitudes A_{rel} and A_{imp} were $3.21(1)\%$ and $1.8(1)\%$ respectively, suggesting a significant fraction of muons had not stopped in KBF_4 .

4. Conclusion

Here we have shown that the distinctive evolution of the muon polarisation in the model fluorides KPF_6 and KBF_4 can be used to deduce muon sites to a very high degree of accuracy, and calculating sites this way tends to be much faster than a full DFT+ μ calculation⁷. In addition, we have shown that the nature of the muon site in polyatomic ions tends to be of the type that bridges two separate ions, which appears to be due to the central atom having a strong positive charge. In particular, for KBF_4 the muon site appears to be analogous to the way in which Lewis bases interact with BF_3 ions, a reaction which can be observed by a careful analysis of F– μ –F states, and similar interactions may also occur in other compounds.

These results have strong implications for the study of molecular magnets: often $[\text{BF}_4]^-$ or $[\text{PF}_6]^-$ ions are used as anions to separate the magnetic cations in these systems, which have been studied extensively with μSR [22, 23]. Owing to their complicated nature it has been very difficult to accurately determine the muon sites in these compounds and hence get a full understanding of the way in which the muon perturbs the host. These compounds may even have multiple muon sites, but as each of these would have a distinctive muon polarisation, methods akin to these presented here will be easily applicable by fitting the data to various combinations of likely muon sites.

Acknowledgements

The authors gratefully acknowledge the Science and Technology Facilities Council (STFC) for access to muon beamtime at the ISIS Neutron and Muon Source, UK [24]. The computational work was undertaken using the Advanced Research Computing (ARC) and the Redwood cluster at the University of Oxford, and we acknowledge Jonathan Patterson for support in using the latter facility. J. M. W and S. J. B acknowledge the Engineering and Physical Sciences Research Council (EPSRC) for funding this project.

References

- [1] Bernardini F, Bonfà P, Massidda S and De Renzi R 2013 *Phys. Rev. B* **87** 115148
- [2] Möller J S, Ceresoli D, Lancaster T, Marzari N and Blundell S J 2013 *Phys. Rev. B* **87** 121108(R)
- [3] Churchard A J, Derzsi M, Jagličić Z, Remhof A and Grochala W 2012 *Dalton Trans.* **41** 5172
- [4] Reger D L, Little C A, Rheingold A L, Lam M, Liable-Sands L M, Rhagitan B, Concolino T, Mohan A, Long G J, Briois V and Grandjean F 2001 *Inorg. Chem.* **40** 1508
- [5] Chiu C C, Cheng M C, Lin S H, Yan C W, Lee G H, Chang M C, Lin T S and Peng S M 2020 *Dalton Trans.* **49** 6635
- [6] Yu Y, Honda Z, Katsumata K, Ohishi T, Manabe T and Yamashita M 1996 *Mol. Cryst. Liq. Cryst.* **286** 121
- [7] Steele A J, Lancaster T, Blundell S J, Baker P J, Pratt F L, Baines C, Conner M M, Southerland H I, Manson J L and Schlueter J A 2011 *Phys. Rev. B* **84** 064412
- [8] Fitch A N and Cockcroft J K 1992 *Phase Transitions* **39** 161
- [9] Cockcroft J K 1985 *Neutron-scattering studies of order-disorder transitions in hexafluoride salts ABF_g* Ph.D. thesis University of Oxford
- [10] Giblin S R, Cottrell S P, King P J C, Tomlinson S, Jago S J S, Randall L J, Roberts M J, Norris J, Howarth S, Mutamba Q B, Rhodes N J and Akeroyd F A 2014 *Nucl. Instrum. Methods Phys. Res., Sect. A* **751** 70
- [11] Wilkinson J M and Blundell S J 2020 *Phys. Rev. Lett.* **125** 087201
- [12] Wilkinson J M, Pratt F L, Lancaster T, Baker P J and Blundell S J 2021 *Phys. Rev. B* **104** L220409

⁷ Each DFT+ μ run takes around 2 days using 64 cores on a cluster, whereas the muon polarisation for a system with a Hilbert space of dimension 2048×2048 takes around eight seconds on a standard PC.

- [13] Bonfà P, Frassinetti J, Wilkinson J M, Prando G, Isah M M, Wang C, Spina T, Joseph B, Mitrović V F, De Renzi R, Blundell S J and Sanna S 2022 *Phys. Rev. Lett.* **129** 097205
- [14] Lang M, Müller J, Steglich F, Brüuhl A, Wolf B and Dressel M 2004 *J. Phys. IV France* **114** 111
- [15] Brunton G 1969 *Acta Crystallogr., Sect. B: Struct. Sci* **25** 2161
- [16] Lucken E A C 1969 *Nuclear quadrupole coupling constants*, (London; New York: Academic P.)
- [17] Langhoff P W and Hurst R P 1965 *Phys. Rev.* **139** A1415
- [18] Lahiri J and Mukherji A 1966 *Phys. Rev.* **141** 428
- [19] Dalgarno A 1962 *Adv. Phys.* **11** 281
- [20] Grabowski S J 2015 *ChemPhysChem* **16** 1470
- [21] Hirao H, Omoto K and Fujimoto H 1999 *J. Phys. Chem. A* **103** 5807
- [22] Lancaster T, Blundell S J, Baker P J, Brooks M L, Hayes W, Pratt F L, Manson J L, Conner M M and Schlueter J A 2007 *Phys. Rev. Lett.* **99** 267601
- [23] Manson J L, Conner M M, Schlueter J A, Lancaster T, Blundell S J, Brooks M L, Pratt F L, Papageorgiou T, Bianchi A D, Wosnitza J and Whangbo M H 2006 *Chem. Commun.* (47) 4894–4896
- [24] Data will be made available at the URL <https://doi.org/10.5286/ISIS.E.RB1920547>